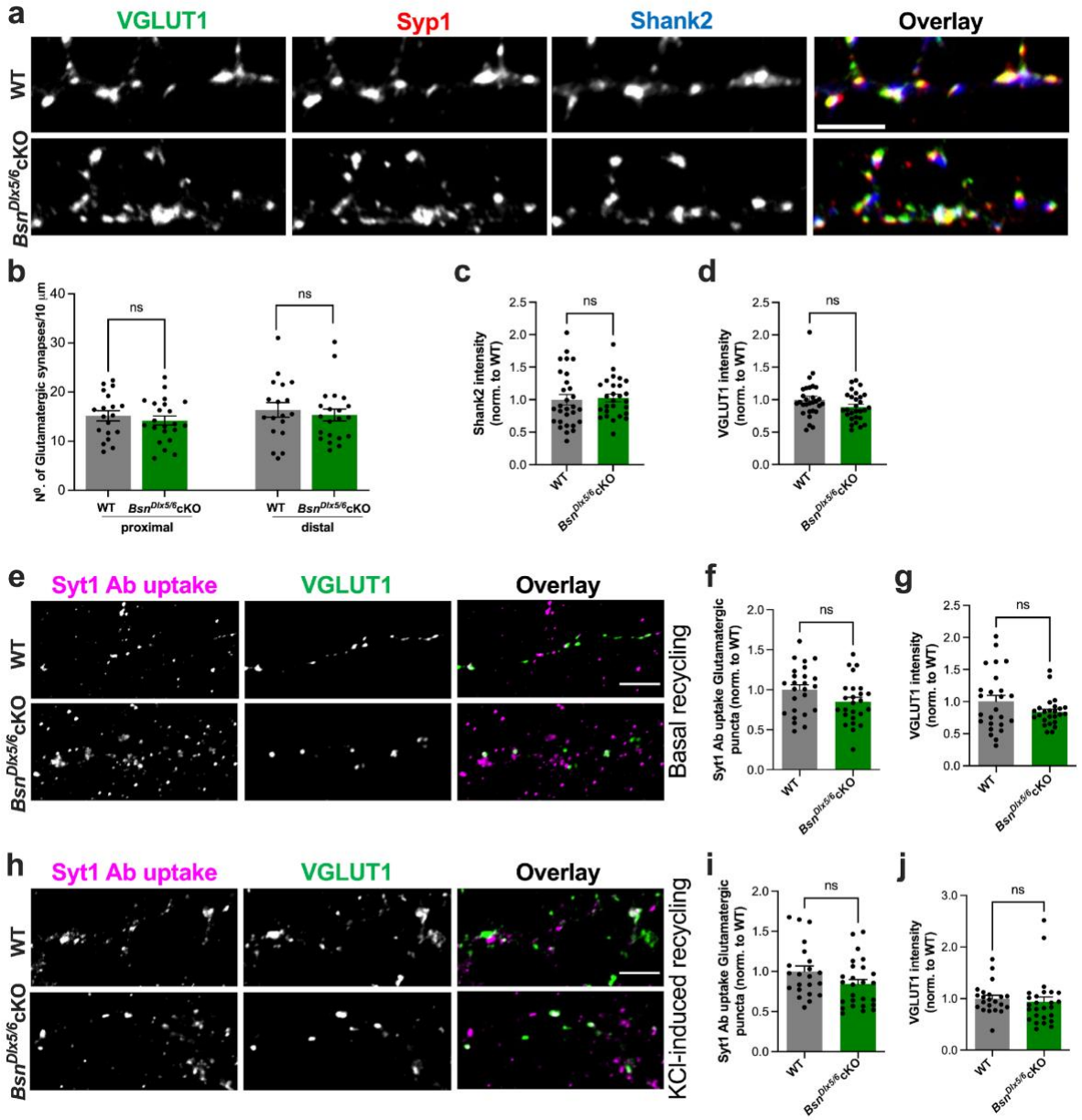

Supplementary Figure S1.

Unaltered synapse density and function of excitatory synapses in *Bsn*$^{Dlx5/6}$cKO hippocampal cultures. a) Representative images of 19-21 DIV cultured hippocampal neurons from WT and Bsn$^{Dlx5/6}$cKO immunostained for VGLUT1, Syp1, and Shank2 to label excitatory synapses. **b)** Quantification of the number of excitatory synapses per 10 µm in the proximal and distal dendritic segments reveal no significant change between genotypes. Proximal: t(39)=0.697; distal: U=165) **c,d)** Quantification of normalized IF intensity for Shank2 [**c**; t(54)=0.262] and VGLUT1 (**d;** U=320) also reveal no significant changes. Data are obtained from 2 independent cultures per condition. **e**) Representative images of Syt1Ab uptake (magenta) driven by endogenous network activity in hippocampal neurons 19-21 DIV from *WT* and *Bsn*$^{Dlx5/6}$*cKO* mice. VGLUT1 (green) marks the excitatory synapses. **f)** Quantification of normalized immunofluorescence of Syt1Ab in excitatory synapses from experiments shown in panel in e. **g)** Quantification of immunofluorescence intensity for VGLUT1 shows

no changes in the *Bsn*$^{Dlx5/6}$*cKO* neurons. Basal recycling: t(48)=1.840; VGLUT1 intensity: U=271. **h)** Representative images of Syt1Ab uptake (magenta) upon depolarization with 50mM KCl. Culture and staining conditions identical to panel e. **i)** Quantification of normalized immunofluorescence of Syt1Ab uptake in excitatory synapses in experiments shown in panel h. **j)** Quantification of immunofluorescence intensity for VGLUT1 on experiments from panel h. Evoked recycling: U=204; VGLUT1 intensity: U=224. Data are obtained from 3 independent culture preparations. All values are mean ± SEM. **P* ≤ 0.05, ***P* ≤ 0.01, ****P* ≤ 0.001. Student's *t*-test, Scale bars, 5 µm.

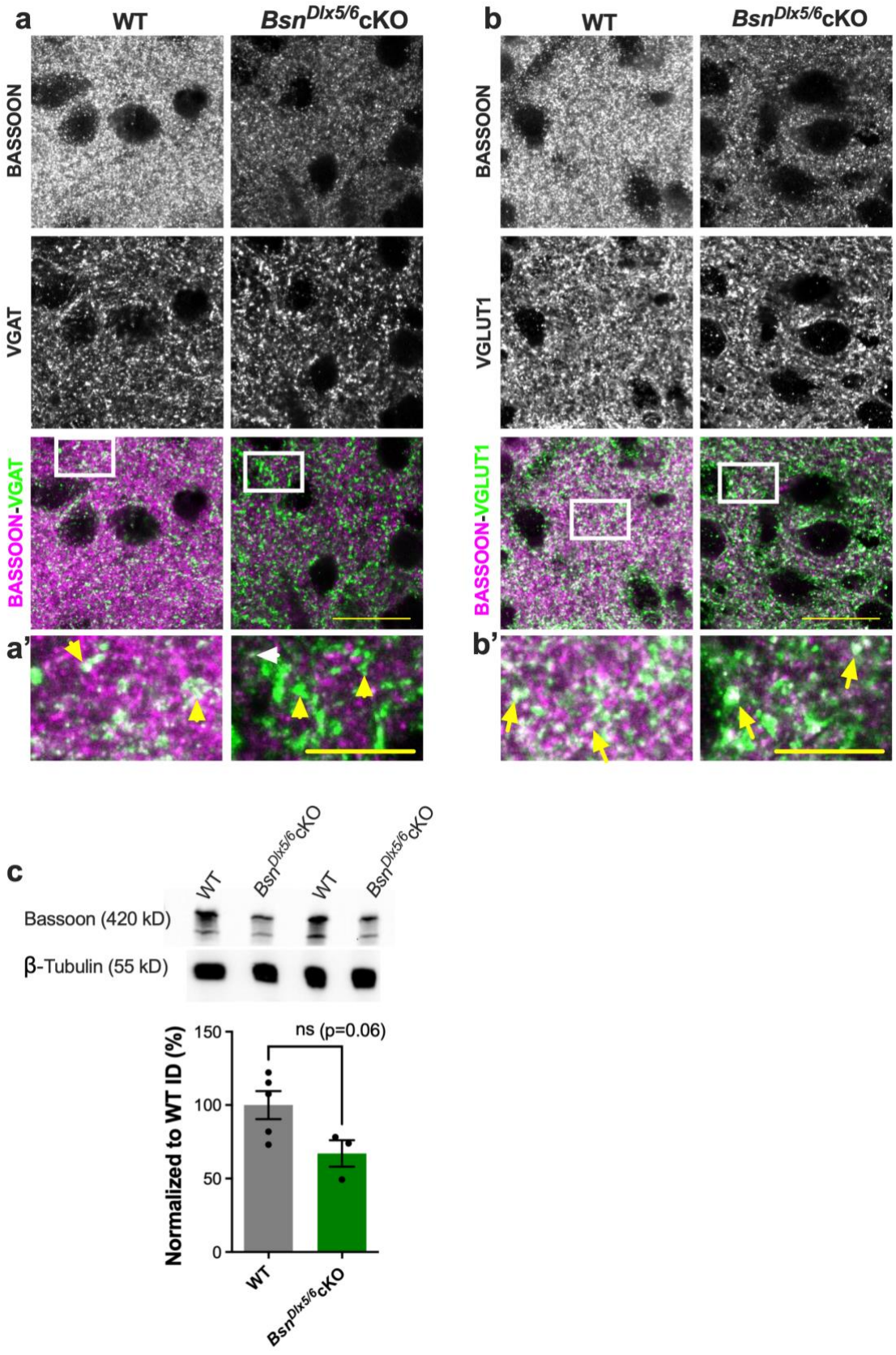

Supplementary Figure S2.

Characterization of Bassoon expression in brains of *Bsn*$^{Dlx5/6}$cKO mice. a) Striatal sections from WT and *Bsn*$^{Dlx5/6}$cKO mice are stained with antibodies against Bassoon and VGAT. **a')** Magnified

overlay images showing colocalization of Bassoon and VGAT in WT, and much less so in *Bsn*$^{Dlx5/6}$cKO sections, as indicated by yellow arrow heads. Remaining expression of Bassoon in some of the VGAT positive synapses of *Bsn*$^{Dlx5/6}$cKO is indicated by white arrow heads. **b)** Striatal sections stained with antibodies against Bassoon and VGLUT1. **b')** Magnified overlay images documenting profound colocalization between Bassoon and VGLUT1 immunoreactivities in both the genotypes (indicated by arrows). Scale bar in **a** and **b** are 25 µm and in **a'** and **b'** is 10 µm. **c)** Representative Western blot showing Bassoon and β-Tubulin (loading control) immunoreactivity analyzed using forebrain tissue from WT (N=5) and *Bsn*$^{Dlx5/6}$cKO (N=3) mice and the respective quantification of the signal [WT: 100 ± 9.583%; *Bsn*$^{Dlx5/6}$cKO: 67.12 ± 8.998%; Student's *t*-test t(6)=2.289]. Values are mean ± SEM.

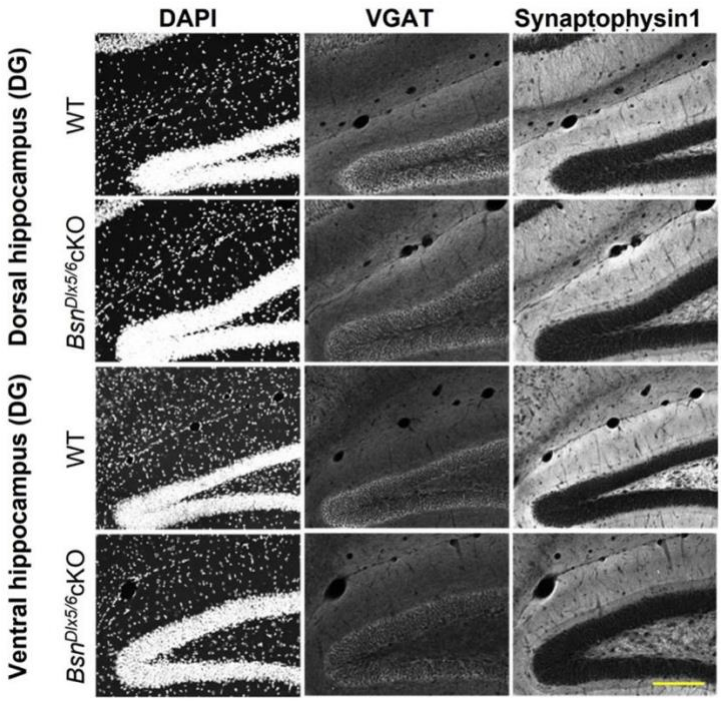

Supplementary Figure S3.

Immunohistochemical analysis of VGAT and Synaptophysin1 expression in *Bsn*$^{Dlx5/6}$cKO brains. Representative images from WT and *Bsn*$^{Dlx5/6}$cKO mice showing staining patterns of VGAT and Synaptophysin1 in dorsal and ventral hippocampal sections (dentate gyrus, DG, is shown as an example). DAPI staining is used to define the cellular layers like the granule cell layer in DG and pyramidal layers in CA3 and CA1, to analyze the VGAT and Synaptophysin1 intensities. Scale bar is 200 µm.

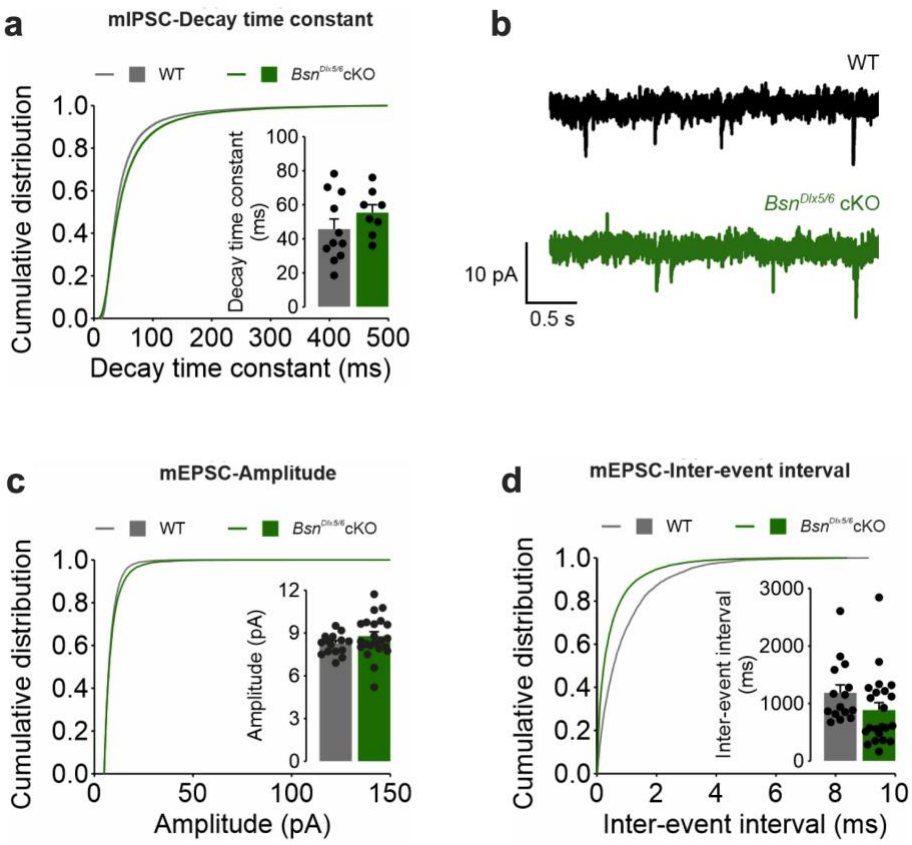

Supplementary Figure S4.

Unaltered mEPSC in the ventral CA1 pyramidal neurons of *Bsn*$^{Dlx5/6}$cKO mice. a) Cumulative distribution of the decay time constant of the recorded mIPSCs. (Inset) mean ± SEM of the average mIPSC decay time constant of individual recorded cells [WT: 45.68 ± 5.95 ms; n=11 cells in N=3 mice; *Bsn*$^{Dlx5/6}$cKO: 55.37 ± 4.66 ms; n=8 cells from N=3 mice; t(17) =-1.203, p=0.245]. **b)** Representative traces of mEPSC recordings of vCA1 PCs from WT (black) and *Bsn*$^{Dlx5/6}$cKO (green) animals. **c)** Cumulative distribution of the amplitude of mEPSCs recorded in pyramidal cells of the ventral CA1. (Inset) Barplot showing the mean ± SEM of the average mEPSC amplitude values of individual recorded cells [WT: 8.27 ± 0.18 pA; n=15 cells from N=7 animals; *Bsn*$^{Dlx5/6}$cKO: 8.78 ± 0.31 pA; n=22 cells from N=6 animals; t(17)=-1.250, p=0.22]. **d)** Cumulative distribution of the inter-event intervals of the recorded mEPSCs. (Inset) Mean ± SEM of the average mEPSC inter-event interval values of individual recorded cells (WT: 1185.45 ± 138.24 ms; n=15 cells from N=7 animals; *Bsn*$^{Dlx5/6}$cKO: 884.17 ± 130.59 ms; n=22 cells from N=6 animals; U=103, Mann-Whitney *U*-test).

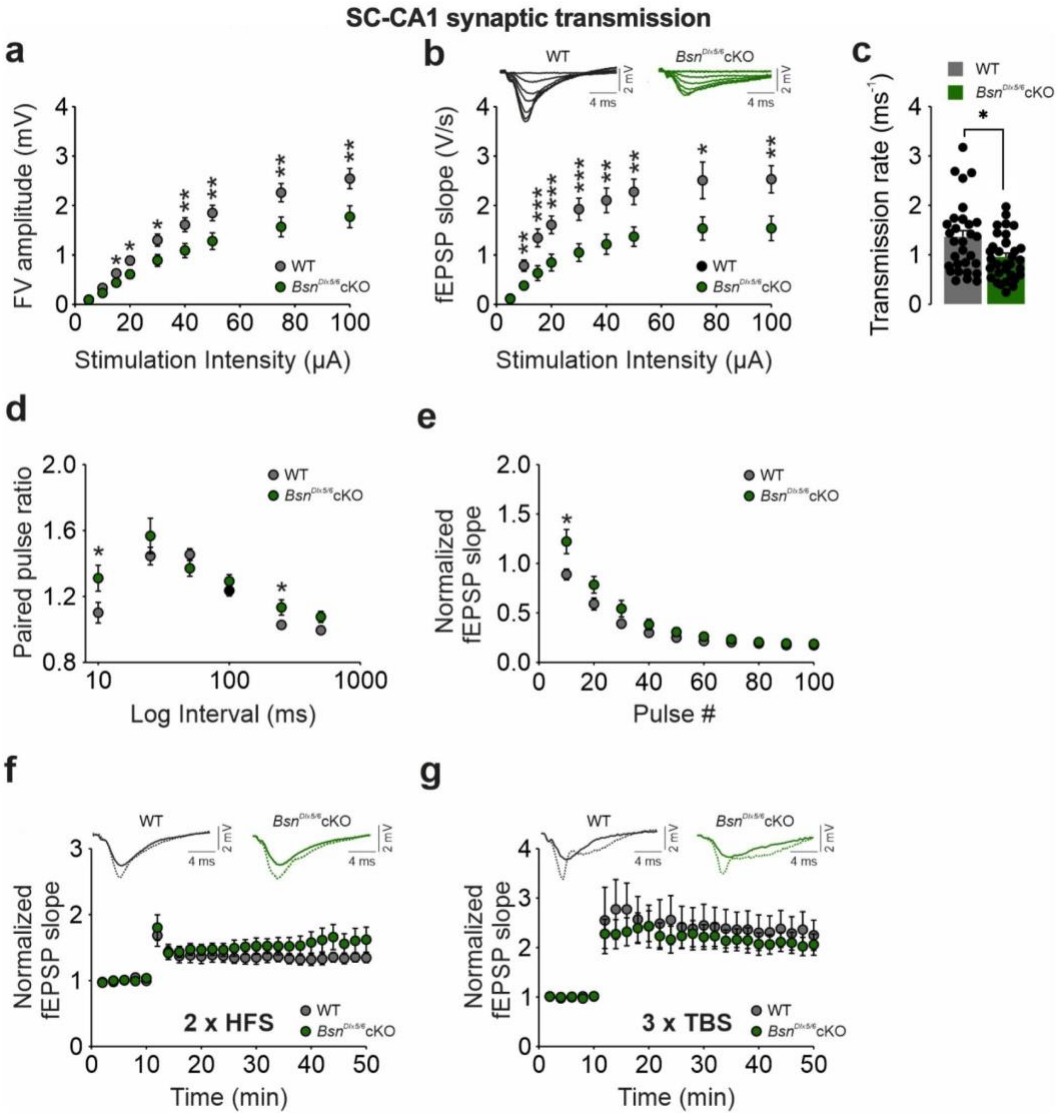

Supplementary Figure S5.

Reduced baseline transmission and enhanced short-term plasticity at the ventral SC-CA1 synapse of *Bsn*$^{Dlx5/6}$ cKO mice. a) Input-output (I-O) curves showing reduced FV responses (WT: N=11 mice, n=32 slices; cKO: N=11 mice, n=33 slices) and **b)** reduced fEPSP responses at the ventral SC-CA1 synapse of *Bsn*$^{Dlx5/6}$ cKO mice (WT: N=11 mice, n=32 slices; cKO: N=11 mice, n=34 slices). **c)** Summary graph indicating a reduced synaptic efficacy (reduced transmission rate per slice) at the ventral SC-CA1 synapse of cKO mice (WT: N=11 mice, n=32 slices; cKO: N=11 mice, n=33 slices). Summary graphs showing **d)** increased paired-pulse ratios (WT: N=11 mice, n=33 slices; cKO: N=11 mice, n=34 slices) at specific intervals (10 ms and 250 ms) accompanied by **e)** a mildly reduced synaptic fatigue during HFS (WT: N=4 mice, n=11 slices; cKO: N=4 mice, n=9 slices) in the ventral CA1 of *Bsn*$^{Dlx5/6}$ cKO mice. Summary graphs demonstrating no change in the **f)** HFS-induced LTP [WT: N=4 mice, n=8 slices; cKO: N=4 mice, n=7 slices; t(13)=-1.455] and **g)** TBS-induced LTP (WT: N=7 mice, n=17 slices; cKO: N=7 mice, n=20 slices; U=168). Data are presented as mean ± SEM. **a, b:** Mann-Whitney *U*-test or Student´s two-tailed test for each stimulation intensity; **d:** Mann-Whitney *U*-test or Student´s two-tailed test for each stimulus interval; **e:** Student´s two-tailed test for each block of pulses;

c: Mann-Whitney *U*-test; **f:** Student´s two-tailed test; **g:** Mann-Whitney *U*-test**.** **P* ≤ 0.05, ***P* ≤ 0.01, ****P* ≤ 0.001.

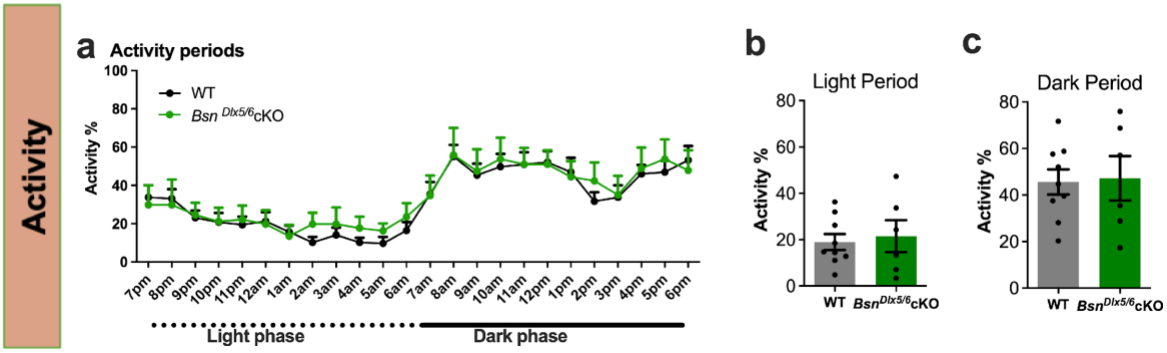

Supplementary Figure S6.

Unaltered home cage activity in *Bsn*$^{Dlx5/6}$cKO mice. a) WT (N=9) and *Bsn*$^{Dlx5/6}$cKO (N=6) display the expected circadian activity differences, with increased locomotion during the dark phase. No genotype differences are apparent [F(23,299)=30.24; genotype effect: [F(1,13)=0.06; genotype x daytime interaction [F(23,299)=0.66]. **b,c)** Unaltered average activity during light (Light phase activity (%) WT: 19.00 ± 3.452, cKO: 21.53 ± 6.908) and dark period between genotypes (dark phase activity (%) WT: 45.62 ± 5.389, cKO: 47.22 ± 9.577). Values are mean ± SEM; two-way repeated measures ANOVA with Bonferroni post-test, Student's *t*-test.

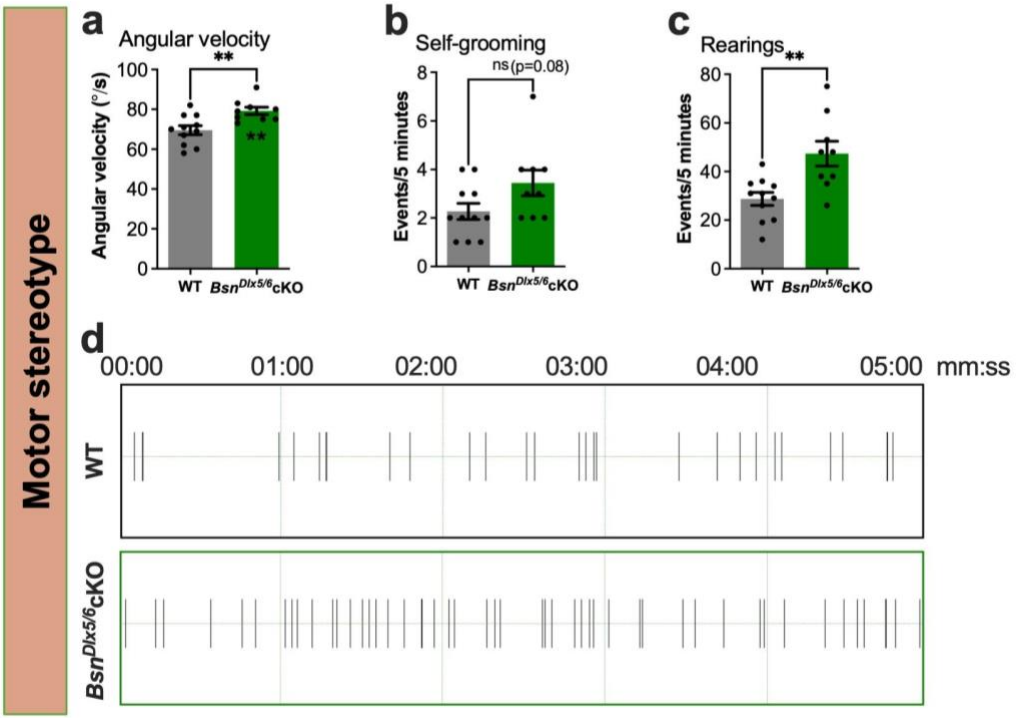

Supplementary Figure S7.

Altered motor patterns of *Bsn*$^{Dlx5/6}$cKO mice in the open field arena. a) *Bsn*$^{Dlx5/6}$cKO mice (N=9) display increased angular velocity compared to WT mice (N=11) [t(18)=3.221, Student's *t*-test] and **b)** non-significant trend for an increase in self-grooming events (U=27, Mann–Whitney *U*-test). **c)** Increased rearing events (including rearings at the walls and free rearings) in *Bsn*$^{Dlx5/6}$cKO mice compared to WT mice **[**t(18)=3.390]. **d)** Representative event chart demonstrating the generally reduced inter-event-intervals of rearings in *Bsn*$^{Dlx5/6}$*cKO* mice. Values are mean ± SEM; **P* ≤ 0.05, ***P* ≤ 0.01, Student's *t*-test, Mann-Whitney *U*-test.

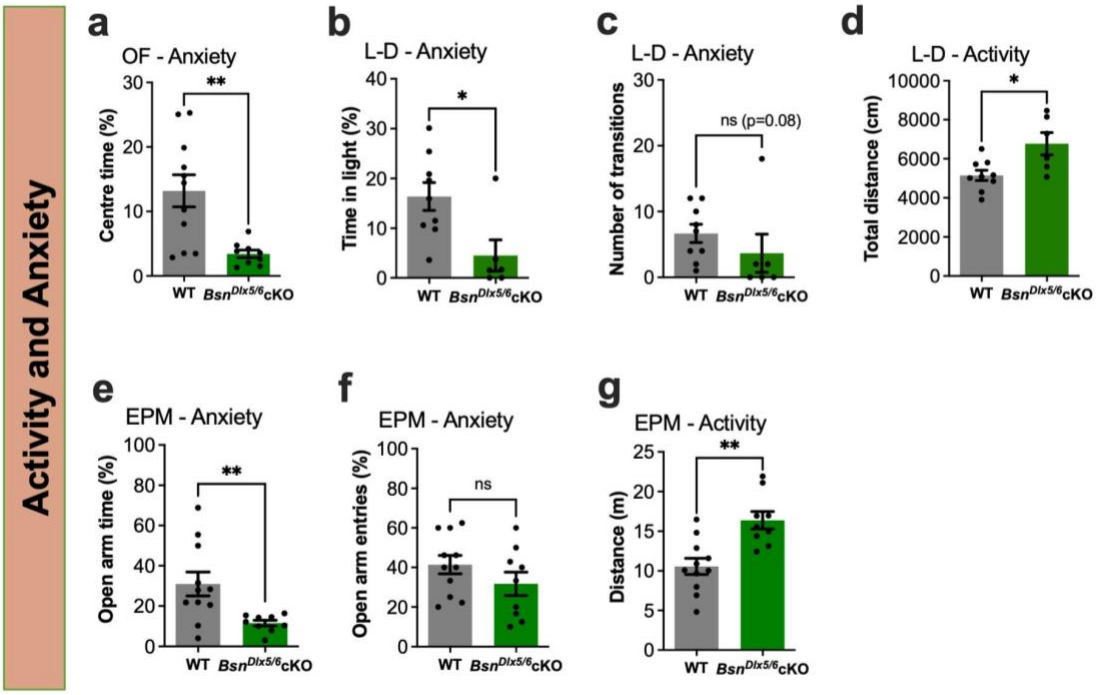

Supplementary Figure S8.

Increased activity and anxiety in *Bsn*$^{Dlx5/6}$cKO mice. a) Decreased time spent by *Bsn*$^{Dlx5/6}$cKO mice (N=9) in the center region of the open field, indicating increased anxiety-like behavior compared to WT mice (N=11) center time (%): t(18)=3.470]. To control for potential effects of hyperlocomotion, we performed a linear regression analysis using locomotor activity as a covariate. The relationship between locomotion and anxiety-like behavior did not differ between groups (slopes: F(1,16)=0.23, p=0.64). After adjusting for locomotion, the group effect was reduced and did not reach statistical significance (intercepts: F(1,17)=4.02, p=0.061), although a strong trend remained. These results indicate that increased locomotion may partially contribute to the observed anxiety phenotype. **b, c)** *Bsn*$^{Dlx5/6}$cKO mice (N=6) spent reduced time (U=9) in the illuminated compartment, and fewer transitions between light and dark compartments of the L-D arena (U=21.50) compared to WT mice (N=9). **d)** Further, *Bsn*$^{Dlx5/6}$cKO mice display increased total activity compared to WT mice, during the L-D test [t(13)=2.877]. **e)** During the elevated plus maze test, *Bsn*$^{Dlx5/6}$cKO mice (N=9) spent less time (%) in the open arm [t(18)=2.899], compared to WT mice (N=11). The relationship between locomotion and anxiety-like behavior did not differ between groups (slopes: F(1,16)=2.78, p=0.11), validating the assumption of homogeneity. After adjusting for locomotion, the group effect was unaltered (intercepts: F(1,17)=0.50, p=0.49), thus indicating a little or no influence of locomotion towards the observed anxiety phenotype in cKO in this test. **f, g)** Further, *Bsn*$^{Dlx5/6}$cKO mice display non-significant change in open arm entries (%) [t(18)=1.309], and increased total activity [t(18)=3.880]. All values are mean ± SEM; *$P \leq 0.05$, **$P \leq 0.01$, Student's *t*-test, Mann-Whitney *U*-test.

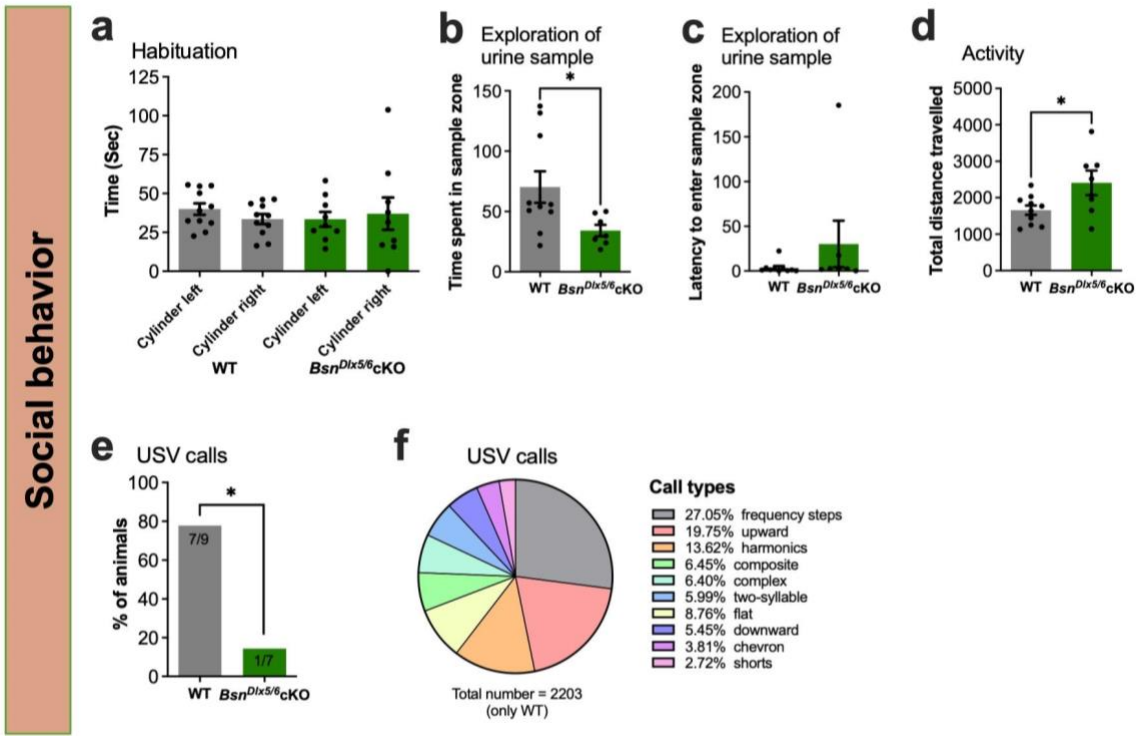

Supplementary Figure S9.

Disturbance of social behavior of *Bsn*$^{Dlx5/6}$cKO mice. a) During the habituation phase of a 3-chamber social test, both WT (N=11) and *Bsn*$^{Dlx5/6}$cKO (N=9) mice explore the empty cylinders equally long [WT: t(10)=1.033; *Bsn*$^{Dlx5/6}$cKO: t(8)=0.2874, Student's paired *t*-test]. **b-d)** When exposed to urine of female mice in estrus *Bsn*$^{Dlx5/6}$cKO (N=7) mice spend less time in the quarter of the sample zone compared to WT mice (N=9) (U=10, Mann–Whitney *U*-test). This is not related to any difference in the latency to enter this zone, which is unaltered between genotypes (U=23). However, again, an enhanced locomotor activity of *Bsn*$^{Dlx5/6}$cKO mice is observed during this exposure session [t(15)=2.36]. **e)** During exposure to female mice in estrus, the proportion of sessions with ultrasonic vocalization (USV) is significantly reduced in *Bsn*$^{Dlx5/6}$cKO mice (1 out of 7 mice elicit USV calls) compared to WT (7 out of 9 mice) (χ^2=6.35, Chi-square test). **f)** Classification of the call types in the sessions with WT mice. The most prominent call types are frequency steps (27%), upward (20%) and harmonics (14%). All values are mean ± SEM; *$P \leq 0.05$, Student's *t* test, Mann-Whitney *U*-test, χ^2-test.

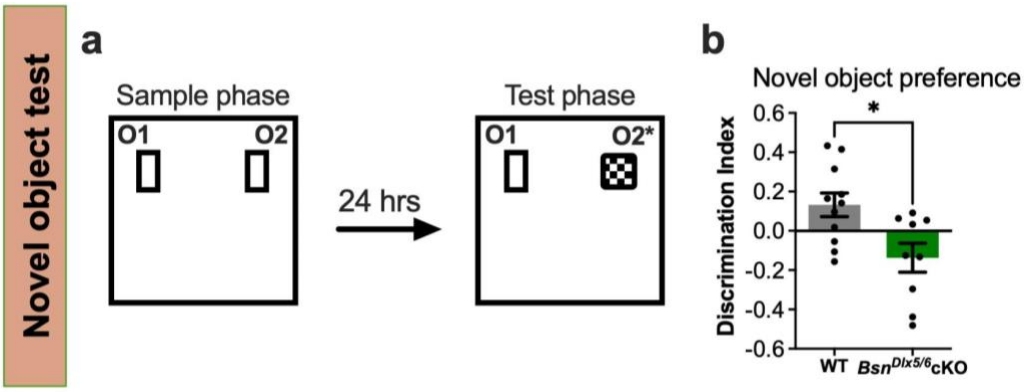

Supplementary Figure S10.

Reduced novel object exploration in *Bsn*$^{Dlx5/6}$cKO mice. a) Schematic representation of novel object recognition test. **b)** During the test phase, cKO mice display negative discrimination index indicating no preference for but rather avoidance of the novel object relative to familiar object [Discrimination index: t(18)=2.858]. All values are mean ± SEM; **P* ≤ 0.05, 2-way repeated measures ANOVA; Student's *t*-test.

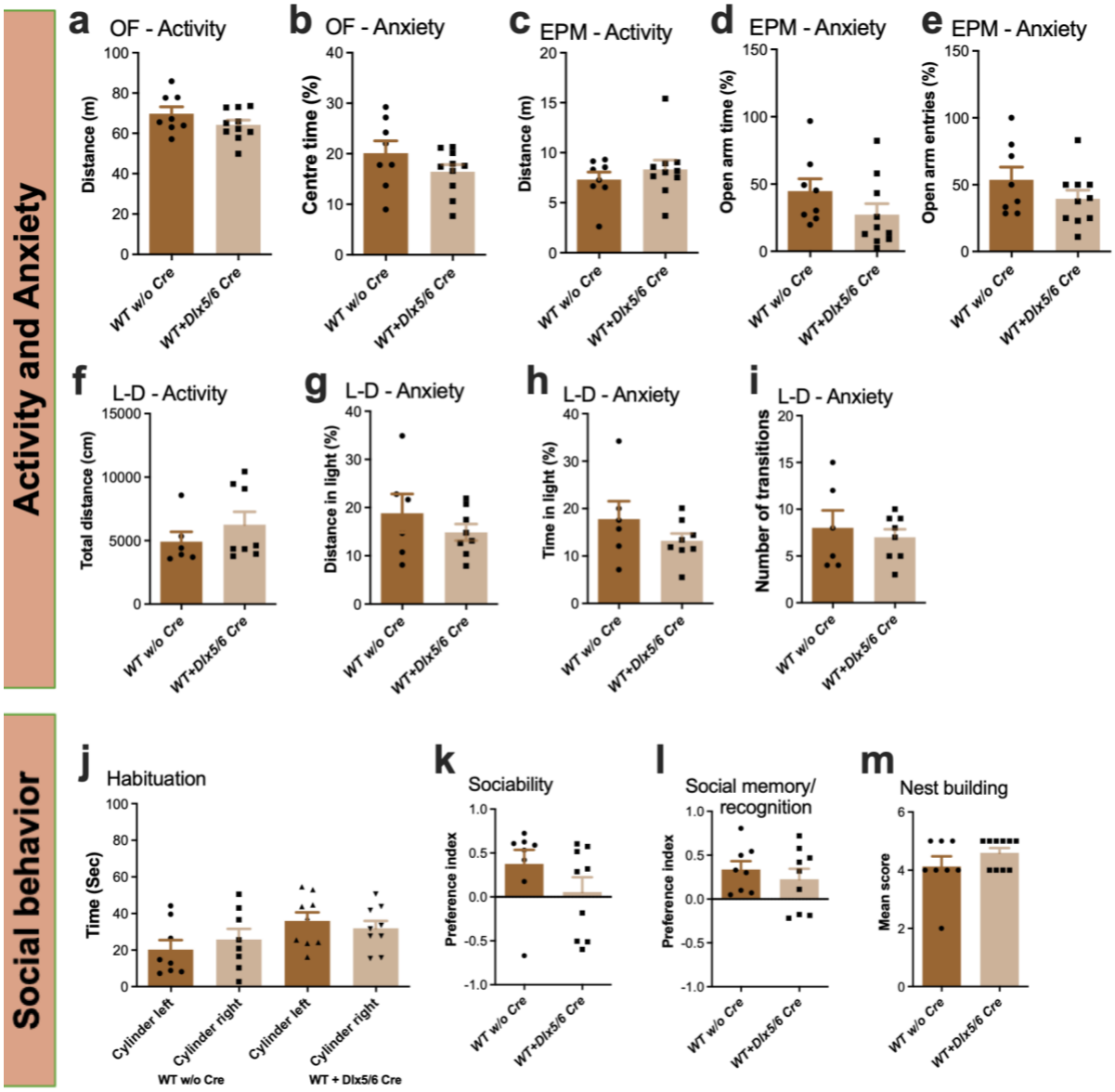

Supplementary Figure S11.

No effect of expression of Dlx5/6-Cre transgene on *Bsn* wildtype background on the behavioral phenotype. a) In open field, *Bsn*$^{+/+}$ (**WT w/o Cre**; N=8); and *Bsn*$^{+/+}$ *X Tg(dlx5a-cre)* (**WT + Dlx5/6Cre**): N=10), display comparable exploratory behavior [t(16)=1.375, p=0.1882, Student's *t*-test]. **b)** In the open field both the groups display comparable anxiety levels [t(16)=1.371, p=0.1893. **c)** Total distance covered in EPM is not altered between the groups [t(16)=0.8207, p=0.4239]. **d,e)** The open arm time (%) [t(16)=1.425, p=0.1733], and open arm entries (%) [t(16)=1.270, p=0.2222] are unchanged between the groups. **f)** Groups show equal total locomotor activity during the L-D test (U=15, p=0.2824, Mann–Whitney *U*-test) and **g,h,i)** comparable anxiety levels [distance: t(12)=0.9963, p=0.3388; duration: t(12)=1.243, p=0.2375; transitions: t(12)=0.5272, p=0.6076] in the illuminated chamber, indicating no change in anxiety-like behavior due to Cre insertion. **j)** Social behavior analyzed in a 3-chambered test. During habituation, the groups spent equal time exploring the empty cylinders [*Bsn*$^{+/+}$: t(7)=0.8565, p=0.4201; *Bsn*$^{+/+}$*X Tg(dlx5a-cre)*: t(8)=0.4855, p=0.6403 Student's paired *t*-test]. **k,l)** No genotype difference in the preference for the conspecific stranger (#1) during the sociability test over a non-

animated object [t(15)=1.368, p=0.1914] and for a novel stranger (#2) over familiarized conspecific #1 during the social memory or recognition test [t(15)=0.7203, p=0.4824], suggesting no obvious social phenotype among *Dlx5/6* control groups. **m)** The groups scored equally in building a quality nest (U=29, p=0.2878). All values are mean ± SEM, Unpaired and paired Student's *t*-test and Mann–Whitney *U*-test.

a **Upregulated proteins: Pathway Enrichment**

Pathway	p-Value (Holm-Bonferroni p 0.05)
The citric acid (TCA) cycle and respiratory electron transport	0.00045
Respiratory electron transport, ATP synthesis by chemiosmotic coupling, and heat production by uncoupling proteins	0.03055
Platelet degranulation	0.03795
Response to elevated platelet cytosolic Ca2+	0.04921

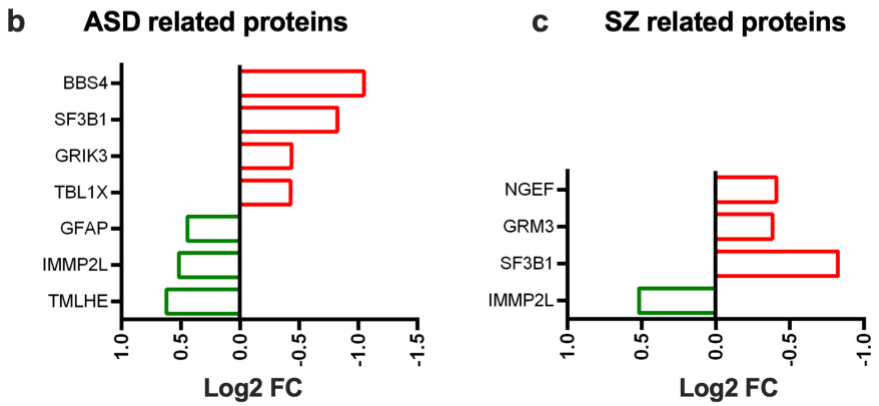

Supplementary Figure S12.

Pathway enrichment and altered ASD / SZ related proteins. a) The pathway enrichment analysis among upregulated proteins in *Bsn*$^{Dlx5/6}$cKO mice, are associated with mitochondrial related functions. **b,c)** List of ASD (SFARI, https://www.sfari.org/) and SZ (http://www.szdb.org) associated proteins significantly regulated (green color-upregulated and red color-down regulated) in *Bsn*$^{Dlx5/6}$cKO mice.

a

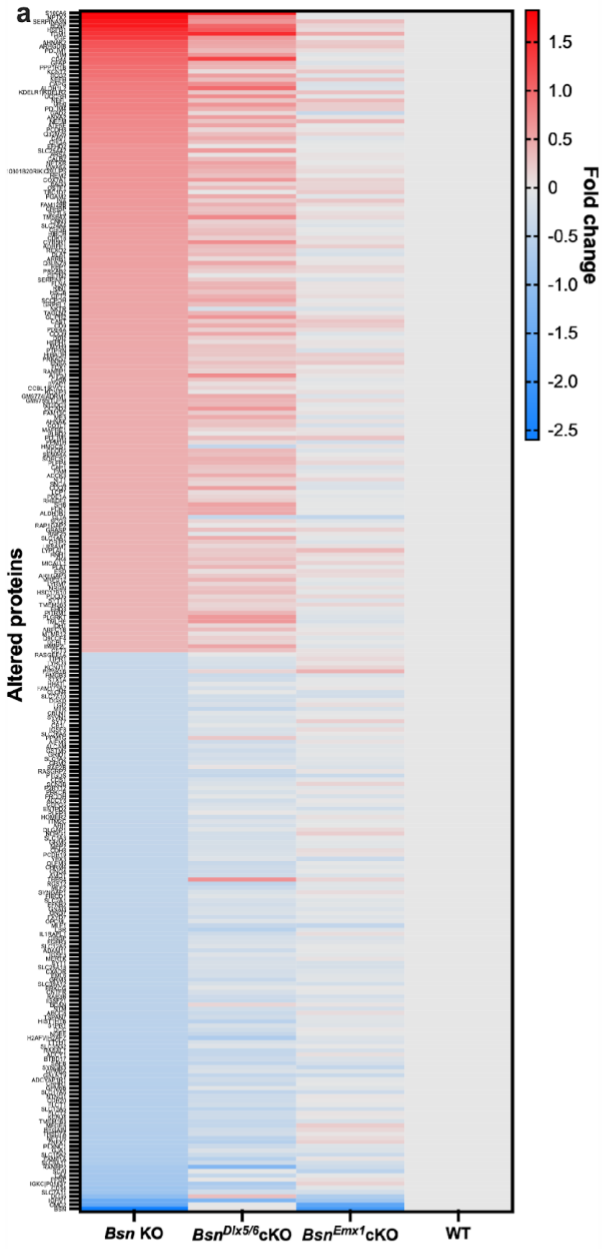

Bsn KO

b GO term: Cellular component

GO Term	GO	p-Value (Holm-Bonferroni p 0.05)
cell junction	GO:0030054	1.387e-31
synapse	GO:0045202	1.311e-30
plasma membrane region	GO:0098590	3.712e-19
plasma membrane bounded cell projection	GO:0120025	1.432e-18
cell projection	GO:0042995	2.314e-18

c GO term: Biological process

GO Term	GO	p-Value (Holm-Bonferroni p 0.05)
trans-synaptic signaling	GO:0099537	7.919e-12
synaptic signaling	GO:0099536	1.232e-11
cell-cell signaling	GO:0007267	1.340e-11
chemical synaptic transmission	GO:0007268	2.600e-11
anterograde trans-synaptic signaling	GO:0098916	2.600e-11

d GO term: Molecular function

GO Term	GO	p-Value (Holm-Bonferroni p 0.05)
transporter regulator activity	GO:0141108	2.965e-3
L-glutamate transmembrane transporter activity	GO:0005313	9.397e-3
channel regulator activity	GO:0016247	9.806e-3
structural constituent of postsynaptic intermediate filament cytoskeleton	GO:0099184	1.648e-2
ion channel regulator activity	GO:0099106	2.834e-2

Bsn^{Emx1}cKO

e GO term: Cellular component

GO Term	GO	p-Value (Holm-Bonferroni p 0.05)
Golgi-associated vesicle	GO:0005798	5.004e-4
cytoskeleton of presynaptic active zone	GO:0048788	6.728e-4
cone cell pedicle	GO:0044316	6.718e-3
presynaptic cytoskeleton	GO:0099569	1.878e-2

f GO term: Biological process

GO Term	GO	p-Value (Holm-Bonferroni p 0.05)
presynaptic active zone assembly	GO:1904071	3.311e-2

g

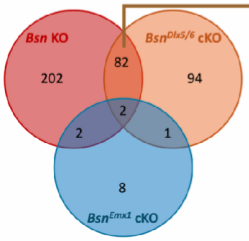

h

Bsn KO and *Bsn*$^{Dlx5/6}$ cKO

GO term: Cellular component

GO Term	GO	p-Value (Holm-Bonferroni p 0.05)
mitochondrion	GO:0005739	3.897e-4
organelle inner membrane	GO:0019866	1.842e-3
mitochondrial inner membrane	GO:0005743	4.525e-3
neuronal dense core vesicle	GO:0098992	4.254e-2

Supplementary Figure S13.

Comparison of proteomic analysis of hippocampal tissue between different Bassoon mouse models. a) Heat-map showing differentially regulated proteins in *Bsn* KO mice and their expression levels in $Bsn^{Dlx5/6}$cKO and Bsn^{Emx1}cKO mice (N=4) normalized to WT (N=4). The color codes fold change (log2) values that indicate an up (in red) or down (blue) regulation of respective proteins (for details see Supplementary Tables S5, S10, S13). A considerable similarity of changes in *Bsn* KO and $Bsn^{Dlx5/6}$cKO is evident with the latter being less pronounced. Clearly less changes are observed in Bsn^{Emx1}cKO mice. **b-d)** *Bsn* KO mice were compared to WT mice in GO cellular component, GO biological processes and GO molecular functions analyses, respectively. Major effects are on synaptic components. **e, f)** Bsn^{Emx1}cKO mice were compared to WT mice in GO cellular component, GO biological processes analyses, respectively. GO terms are mentioned in the order of decreasing enrichment p values (Holm-Bonferroni correction method) and the top 5 GO terms are mentioned here. Again, a strong alteration of the synaptic compartment is evident. **g, h)** Venn diagram showing commonly regulated proteins among all the *Bsn* mutant lines. There are only two proteins (Clathrin light chain A and Immunoglobulin heavy variable1) are common among all the mutant lines, two proteins (Bassoon and Protein SCAI) between *Bsn* KO and Bsn^{Emx1}cKO, only one common protein (Anion exchange protein 2) between $Bsn^{Dlx5/6}$cKO and Bsn^{Emx1}cKO. However, there is a significant overlap among *Bsn* KO and $Bsn^{Dlx5/6}$cKO. Total 82 proteins are commonly regulated which are largely confined to mitochondrial cellular localization.

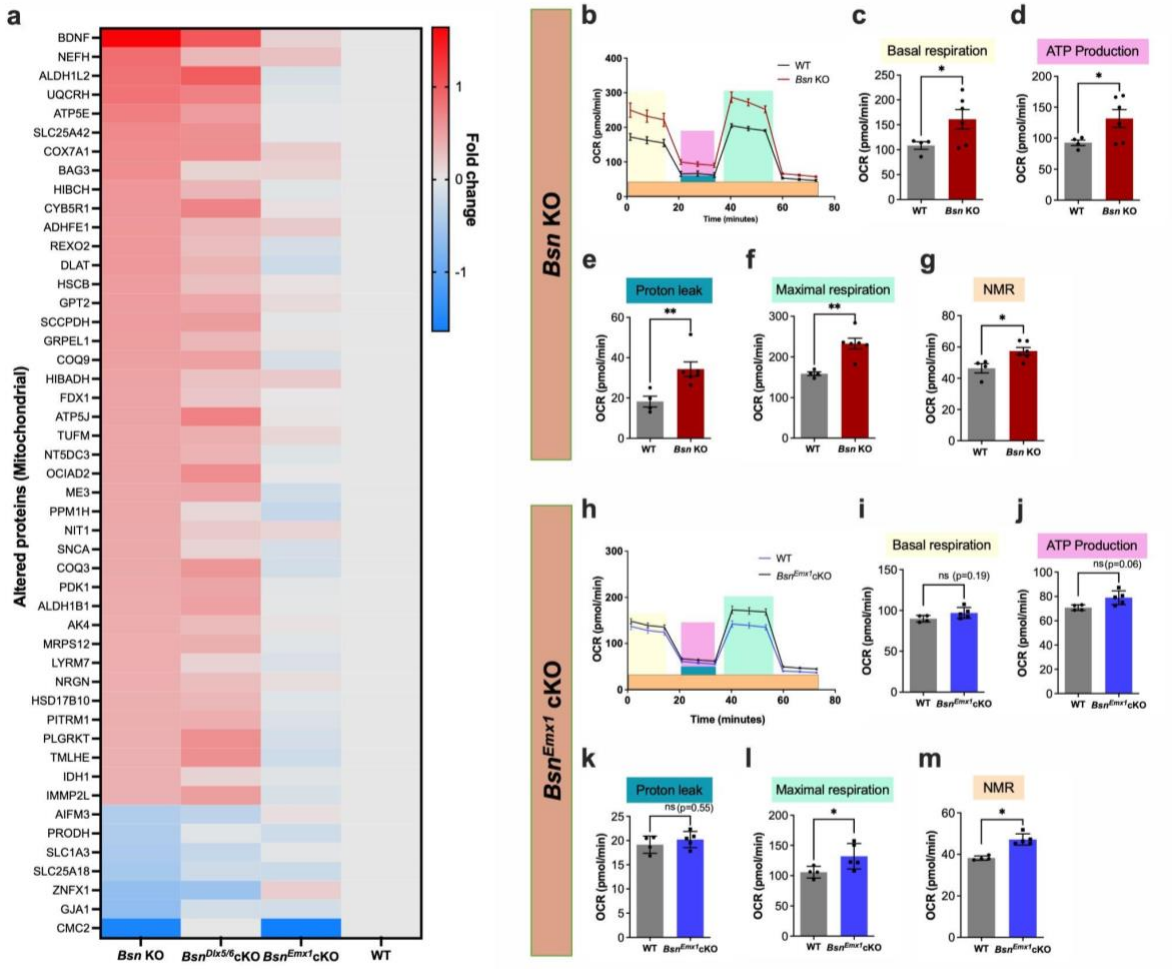

Supplementary Figure S14.

Comparison of mitochondrial proteome analysis and mitochondrial activity between different Bassoon mouse models. a) Heat-map displaying altered mitochondrial proteins in *Bsn*KO mice and their expression levels in *Bsn*$^{Dlx5/6}$cKO and *Bsn*^{Emx1}cKO mice. The color code is a fold change (log2) values that indicates an up (in red) or down (blue) regulation of different proteins. The similarity between *Bsn* KO mice and *Bsn*$^{Dlx5/6}$cKO mice is striking. **b-g)** Real-time mitochondrial respiration (OCR) and key parameters using Seahorse mito stress test on hippocampal neurons from WT and total *Bsn* KO mice. Increased mitochondrial activity, including basal respiration [t(6.4)=2.522], ATP production [t(5.9)=2.593], proton leak [t(8)=3.604], maximal respiration [t(6.1)=5.319], and non-mitochondrial respiration [t(6.4)=2.908], suggests a hyperactive mitochondrion in *Bsn* KO mice, which show patterns similar to those of *Bsn*$^{Dlx5/6}$cKO mice. **h-m)** The same experiments described in (b-g) performed in a conditional mouse line *Bsn*^{Emx1}cKO. There was no statistical difference in most of the key parameters, except for maximal respiration (U=1) and non-mitochondrial respiration (U=0). All values are mean ± SEM; *P ≤ 0.05. **P ≤ 0.01, Unpaired Welch's *t*-test, Mann-Whitney *U*-test.